A&A 677, L15 (2023)
https://doi.org/10.1051/0004-6361/202347329

Astronomy & Astrophysics

LETTER TO THE EDITOR

The GAPS Programme at TNG

XLVII. A conundrum resolved: HIP 66074b/Gaia-3b characterised as a massive giant planet on a quasi-face-on and extremely elongated orbit*

A. Sozzetti[1], M. Pinamonti[1], M. Damasso[1], S. Desidera[2], K. Biazzo[3], A. S. Bonomo[1], D. Nardiello[2], R. Gratton[2], A. F. Lanza[4], L. Malavolta[5], P. Giacobbe[1], L. Affer[6], A. Bignamini[7], F. Borsa[8], W. Boschin[9], M. Brogi[10,1], L. Cabona[2], R. Claudi[2], E. Covino[11], L. Di Fabrizio[9], A. Ghedina[9], A. Harutyunyan[9], C. Knapic[7], J. Maldonado[6], A. Maggio[6], L. Mancini[12,1,13], G. Mantovan[5], F. Marzari[5], S. Messina[4], G. Micela[6], E. Molinari[14], M. Montalto[4], L. Naponiello[12,15,1], I. Pagano[4], M. Pedani[9], G. Piotto[5], E. Poretti[8], G. Scandariato[4], R. Silvotti[1], and D. Turrini[1]

(Affiliations can be found after the references)

Received 30 June 2023 / Accepted 21 July 2023

ABSTRACT

The nearby mid-K dwarf HIP 66074 was recently identified as host to a candidate super-Jupiter companion on a ∼300 day, almost edge-on, orbit, based on *Gaia* Data Release 3 (DR3) astrometry. Initial attempts at confirming the planetary nature of the signal based on publicly available radial-velocity (RV) observations uncovered an intriguing conundrum: the inferred RV semi-amplitude appears to be a factor of 15 smaller than the one predicted based on the *Gaia* solution (corresponding to a 7-$M_{\rm Jup}$ companion on a close to edge-on orbit). We present the results of intensive RV monitoring of HIP 66074 with the HARPS-N spectrograph. We detected the companion at the *Gaia* period, but with an extremely eccentric orbit ($e = 0.948 \pm 0.004$), a semi-amplitude $K = 93.9^{+9.4}_{-7.0}$ m s^{-1}, and a minimum mass $m_{\rm b} \sin i_{\rm b} = 0.79 \pm 0.05\ M_{\rm Jup}$. We used detailed simulations of *Gaia* astrometry with the DR3 time-span to show that the conundrum can be fully resolved by taking into account the combination of the initially sub-optimal RV sampling and systematic biases in the *Gaia* astrometric solution, which include an underestimation of the eccentricity and incorrect identification of orbital inclination, which has turned out to correspond to a close to face-on configuration ($i \lesssim 13°$). With an estimated mass in the approximate range of 3−7 $M_{\rm Jup}$, we find that HIP 66074b (≡Gaia-3b) is the first exoplanet candidate astrometrically detected by *Gaia* to be successfully confirmed based on RV follow-up observations.

Key words. astrometry – planetary systems – planets and satellites: individual: HIP 66074 b – planets and satellites: fundamental parameters – techniques: radial velocities – methods: data analysis

1. Introduction

The publication of *Gaia* Data Release 3 (DR3) on June 13th, 2022 (Gaia Collaboration 2023a) has provided the first catalogue of >800 000 non-single star solutions in the astrometric, spectroscopic, and photometric channels (Gaia Collaboration 2023b). Of these, 169 227 are full, single-Keplerian astrometric orbital solutions (Gaia Collaboration 2023b; Halbwachs et al. 2023). The sample is dominated by solutions with inferred companion masses in the stellar regime, but about 1% of them (1915) corresponds to primaries orbited by objects in the sub-stellar mass regime (assuming zero flux ratio), with 72 companions with estimated masses formally <20 $M_{\rm Jup}$, that is, potentially planetary in nature (Gaia Collaboration 2023b).

The first sample of exoplanet candidates detected by *Gaia* astrometry contains a subset of nine previously known Doppler-detected giant planets, which offered the means for their direct confirmation (Gaia Collaboration 2023b, and references therein). In a few cases, publicly available radial velocity (RV) data were used by Holl et al. (2023) to validate the orbital solutions based on the close correspondence between the values of orbital period obtained from *Gaia* astrometry and the RV data. In this respect, the case of the companion orbiting HIP 66074 (*Gaia* DR3 1712614124767394816) constitutes a rather interesting conundrum. The *Gaia* solution has period $P = 297 \pm 2.8$ d, eccentricity $e = 0.46 \pm 0.17$, inclination $i = 90 \pm 5°$, and angular semi-major axis $a_0 = 0.21 \pm 0.03$ mas. Using a reasonable guess to the mass of its K-dwarf primary, HIP 66074b is inferred to be a super-Jovian planet with $M_{\rm p} \sim 7.0\ M_{\rm Jup}$. Given the large companion mass, for an essentially edge-on orbit the expected RV semi-amplitude K from the *Gaia* solution would be $K \simeq 300$ m s^{-1}. In a work focussed on providing consistency tests between *Gaia* astrometry and Doppler data on selected systems with known and candidate exoplanets, Winn (2022) re-analysed the available Keck HIRES RVs of HIP 66074 (Butler et al. 2017). This work highlighted the presence of an obvious inconsistency: the RV-only solution has the same period of the *Gaia* orbit, but the K-value is 15 times smaller (∼20 m s^{-1}). A combined analysis of the RVs and the *Gaia* solution for the source results in a very good fit, albeit requiring an unrealistically high flux ratio (Winn 2022). A more recent analysis performed by Marcussen & Albrecht (2023) achieved the same conclusions, ruling out the scenario of an astrophysical false positive produced by a binary system with a mass ratio

* Based on observations made with the Italian Telescopio Nazionale *Galileo* (TNG) operated by the Fundación Galileo Galilei (FGG) of the Istituto Nazionale di Astrofisica (INAF) at the Observatorio del Roque de los Muchachos (La Palma, Canary Islands, Spain).

almost equal to the flux ratio, based on the investigation of the public HIRES spectra.

Here, we present an analysis of precise RVs of HIP 66074 gathered at regular cadence with the HARPS-N spectrograph (Cosentino et al. 2012) at the Telescopio Nazionale *Galileo* (TNG) within the context of the programme Global Architecture of Planetary Systems (GAPS, Covino et al. 2013; Desidera et al. 2013). The combination of the new orbital solution and detailed simulations of *Gaia* observations of the system over the DR3 time-span, enabling characterisations of the existing biases in the *Gaia*-only solution, allows us to conclusively confirm the planetary nature of the candidate. Thus, we identified HIP 66074b/Gaia-3b[1] as the first detected exoplanet by *Gaia* astrometry and the first-ever unambiguously confirmed astrometric detection of an exoplanet at any wavelength.

2. Spectroscopic observations

We planned an intensive RV monitoring of HIP 66074 with HARPS-N, collecting a total of 60 spectra between 4 June 2022 and 30 April 2023 (330 days), with a typical exposure time of 900 s. The spectra were reduced with version 3.7.1 of the HARPS-N Data Reduction Software (DRS) pipeline, which is maintained by the Italian centre for Astronomical Archive (IA2)[2]. We derived the RVs using v1.8 of the Template Enhanced Radial velocity Reanalysis Application (TERRA) pipeline (Anglada-Escudé & Butler 2012), particularly suited for late-type dwarfs such as HIP 66074 (Perger et al. 2017). The RV time series obtained with TERRA (reported in Table D.1) has a median of $\sigma_{\rm RV} = 1.25\,{\rm m\,s^{-1}}$ and rms of $22.3\,{\rm m\,s^{-1}}$.

3. Analysis

3.1. Updated stellar parameters

Assuming as the input parameters the effective temperature ($T_{\rm eff}$) and surface gravity ($\log g$) from the StarHorse2 catalogue (Anders et al. 2022), we derived the final $T_{\rm eff}$, $\log g$, and iron abundance ([Fe/H]) using both the spectral synthesis and equivalent width methods to the co-added spectrum of the target. In the first case, we considered the SME code (Piskunov & Valenti 2017; version 2020), while in the second case we considered the MOOG code (Sneden 1973; version 2019) and the iron line list by Biazzo et al. (2022). In both cases, we fixed the microturbulence velocity ξ to $0.5\,{\rm km\,s^{-1}}$ from the relationship by Adibekyan et al. (2012), and we used MARCS (Gustafsson et al. 2008) and ATLAS9-ODFNEW (Castelli & Kurucz 2003) grids of model atmospheres, obtaining consistent results. Moreover, within the spectral synthesis procedure, we adopted the macroturbulence velocity of $1.4\,{\rm km\,s^{-1}}$ by Brewer et al. (2016). We also derived $T_{\rm eff}$ considering the line-depth ratio (LDR) method and appropriate calibrations LDR-$T_{\rm eff}$ developed at the same resolution as HARPS-N (see Biazzo et al. 2011, and references therein). In all three cases, we obtained similar results within the uncertainties. Mean final values of the derived parameters are: $T_{\rm eff} = 4300 \pm 60\,{\rm K}$, $\log g = 4.58 \pm 0.06$, and $[{\rm Fe/H}] = 0.12 \pm 0.05$ (see Table A.1). As a by-product, we also derived through the spectral synthesis technique the projected rotational velocity of $v \sin i_\star = 1.8 \pm 0.6\,{\rm km\,s^{-1}}$. No lithium line was detected in the spectrum, thereby indicating the star is not young.

We derived the stellar mass, radius, and age based on a fit to the star's broad-band spectral energy distribution (SED) from the optical to the mid-infrared (see Fig. B.1) using the EXOFASTv2 code (Eastman 2017; Eastman et al. 2019). The SED fit (see e.g. Stassun & Torres 2016) was performed using archival broad-band *Tycho*-2 and Johnson-Cousins B- and V-band magnitudes, i-band SDSS photometry, 2MASS JHK_s near-infrared magnitudes, and WISE $W1-W4$ IR magnitudes. Within EXOFASTv2 we utilised the YY-isochrones (Yi et al. 2001) to obtain the following stellar properties (also reported in Table A.1): $M_\star = 0.705^{-0.023}_{-0.025}\,M_\odot$, $R_\star = 0.690^{+0.012}_{-0.013}\,R_\odot$, and $t = 7.9^{+4.9}_{-4.1}$ Gyr.

The space velocities support the membership to the thin disk and are well outside the kinematic space of young stars (Montes et al. 2001). These characteristics indicate a plausible age range of ∼2−8 Gyr, consistent with the X-ray non detection in the ROSAT All-Sky Survey. From the HARPS-N spectra we obtained a median Mount Wilson S-index value of $S_{\rm MW} = 0.78$ (the full $S_{\rm MW}$ time-series is reported in Table D.1), corresponding (using the formalism described in Astudillo-Defru et al. 2017) to $\log(R'_{\rm HK}) = -4.80 \pm 0.04$ and an expected rotation period $P_{\rm rot} = 31 \pm 3$ d. This is close to the tentative rotation period of ∼35 d inferred from the analysis of the HARPS-N RV and S-index time series (Sect. 3.2). Such a period is slightly longer than that of stars of similar colour in the 4 Gyr-old open cluster M 67 (Gruner et al. 2023), suggesting an older age. In summary, all the indicators consistently support an old age.

3.2. Spectroscopic orbital solution

We initially fitted a Keplerian orbit to the HARPS-N RV measurements using the publicly available Monte Carlo (MC) nested sampler and Bayesian inference tool `MULTINEST V3.10` (e.g. Feroz et al. 2019), through the `pyMULTINEST` wrapper (Buchner et al. 2014), with uniform priors on the model parameters. The orbital model has the following free parameters: the epoch of inferior conjunction $T_{0,\rm b}$; the orbital period $P_{\rm b}$; a residual RV offset $\gamma_{\rm HN}$; the RV semi-amplitude $K_{\rm b}$; $\sqrt{e_{\rm b}}\cos\omega_{\star,\rm b}$ and $\sqrt{e_{\rm b}}\sin\omega_{\star,\rm b}$, where $e_{\rm b}$ is the eccentricity and $\omega_{\star,\rm b}$ the argument of periastron; an uncorrelated jitter term $\sigma_{\rm jit,HN}$ added in quadrature to the formal uncertainties. We obtained $K \sim 94\,{\rm m\,s^{-1}}$, $P \sim 285$ d, and $e \sim 0.94$. A Generalized Lomb-Scargle (GLS; Zechmeister & Kürster 2009) periodogram analysis of the residuals showed the presence of a peak at ∼35 d, albeit with a high bootstrap-based false alarm probability of ∼11% (Fig. D.1). We performed the same analysis on the S-index time-series, which also returned a clear periodicity at ∼35 d (Fig. D.1, bottom panel). We also downloaded the publicly available photometric data of HIP 66074 from the Mikulski Archive for Space Telescopes (MAST) portal[3] that were gathered by the TESS mission in nine non-consecutive sectors and performed a periodogram analysis of the light curves extracted with an independent pipeline (see e.g. Nardiello et al. 2022). Although TESS observations are not designed to easily detect $P_{\rm rot} > 15$ d, we found evidence of rotational modulation in the range 32−41 d upon inspection of the TESS photometry of different sector subsets, or taken as a whole (Fig. B.2).

Given the convergent view on the likely presence of rotational modulation in the HARPS-N RVs, we then expanded the model to include a stellar activity term using the Gaussian process (GP) regression package `GEORGE` (Ambikasaran et al. 2015) and adopting a quasi-periodic (QP) kernel (see, e.g.

[1] We follow the naming convention for confirmed *Gaia* exoplanets adopted by the Data Processing and Analysis Consortium and presented at https://www.cosmos.esa.int/web/gaia/exoplanets

[2] https://ia2.inaf.it

[3] mast.stsci.edu/portal/Mashup/Clients/Mast/Portal.html

Table 1. Global modelling of the HIP 66074 HIRES and HARPS-N RVs: priors, best-fit, and derived parameters.

Parameter	Prior	Value
Stellar activity – QP kernel (only HARPS-N)		
h [m s^{-1}]	$\mathcal{U}(0, 10)$	$2.9^{+1.5}_{-1.0}$
θ [days]	$\mathcal{U}(32, 37)$	$34.9^{+0.3}_{-0.4}$
λ [days]	$\mathcal{U}(0, 1000)$	603^{+258}_{-293}
ε	$\mathcal{U}(0, 1)$	$0.66^{+0.22}_{-0.28}$
Spectroscopic orbit parameters		
K_b [m s^{-1}]	$\mathcal{U}(0, 200)$	$93.9^{+9.4}_{-7.0}$
P_b [days]	$\mathcal{U}(0, 500)$	$310.9^{+21.7}_{-17.7}$
$T_{0,b}$ [BJD–2 450 000]	$\mathcal{U}(9730, 10\,300)$	9960.2 ± 0.3
$\sqrt{e_b}\sin\omega_{\star,b}$	$\mathcal{U}(-1, 1)$	$-0.414^{+0.032}_{-0.033}$
$\sqrt{e_b}\cos\omega_{\star,b}$	$\mathcal{U}(-1, 1)$	$-0.881^{+0.019}_{-0.017}$
$\sigma_{\rm jit,HN}$ [m s^{-1}]	$\mathcal{U}(0, 20)$	1.6 ± 0.3
$\gamma_{\rm HN}$ [m s^{-1}]	$\mathcal{U}(-100, 100)$	$-7.9^{+2.0}_{-1.8}$
$\sigma_{\rm jit,HIRES}$ [m s^{-1}]	$\mathcal{U}(0, 20)$	$7.6^{+2.9}_{-1.9}$
$\gamma_{\rm HIRES}$ [m s^{-1}]	$\mathcal{U}(-100, 100)$	$-4.0^{+3.1}_{-2.9}$
Derived planetary parameters		
$T_{\rm per,b}$ [BJD–2 450 000]		$9962.48^{+0.07}_{-0.06}$
e_b		0.948 ± 0.004
$\omega_{\star,b}$ [rad]		-2.70 ± 0.04
a_b [au]		$0.799^{+0.035}_{-0.024}$
$m_b \sin i_b$ [$M_{\rm Jup}$]		$0.79^{+0.05}_{-0.04}$

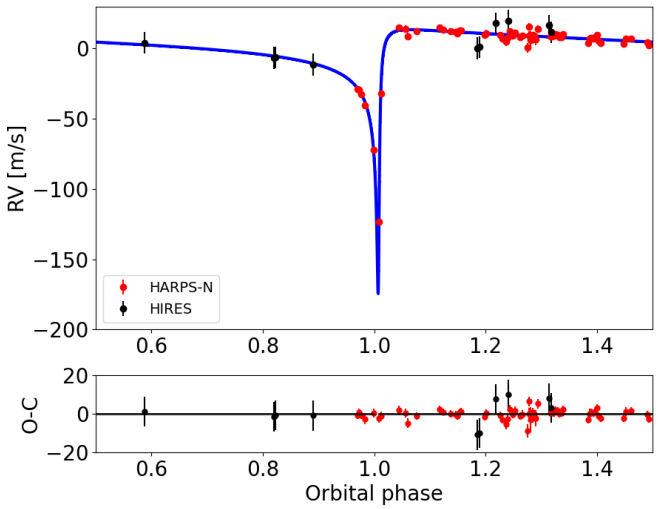

Fig. 1. Phase-folded HIRES and HARPS-N RVs superposed to the best-fit Keplerian orbit (blue curve), calculated using the median values of the posteriors. Phase zero (or phase one) corresponds to the time of inferior conjunction. The residuals of the best-fit model are shown in the bottom panel.

Damasso et al. 2020). We included the publicly available HIRES RVs (omitting, as in Winn 2022, the spectrum gathered at epoch JD = 2455042.76395) in the modelling of the Keplerian signal (requiring the addition of an RV offset $\gamma_{\rm HIRES}$ and an uncorrelated jitter $\sigma_{\rm jit\,HIRES}$ to the set of model parameters); however, the GP QP model was applied only to the HARPS-N RVs, given the sparseness of the former dataset. The combined HARPS-N+HIRES time baseline exceeds 14 years and it is therefore suitable to look for evidence of any long-term RV trends possibly due to long-period companions consistently present in both datasets. In addition to the single Keplerian + GP QP model, we then tested for the presence of acceleration and curvature in the data, but to no avail. The solution with single Keplerian + GP QP is favoured in terms of Bayesian evidence, with marginal likelihood differences of $\Delta \ln \mathcal{Z} > +4$, and we adopted it as fiducial. The priors and final results of the global modelling of the HARPS-N RVs are reported in Table 1, while Fig. 1 shows the best-fit Keplerian solution overplotted to the phase-folded RVs and Figs. E.1 and E.2 show the best-fit solution for the stellar activity component and the full set of joint posteriors, respectively. An inspection of Fig. E.2 shows multiple peaks in the posterior distribution for P. We should keep in mind that the very sparse distribution of HIRES RVs of HIP 66074 (on average, two data points distributed over a full orbital period, never sampling phases close to periastron) is prone to the introduction of period aliases particularly in the case of such a high-eccentricity orbit (see e.g. O'Toole et al. 2009). The results reported in Table 1 seem to indicate coherence of the activity signal (large correlation decay timescale λ) over the time span of the HARPS-N observations. The large value of $\sigma_{\rm jit\,HIRES}$ could possibly be ascribed to unmodeled stellar activity effects in the HIRES RVs.

The outcome of the RV analysis clearly indicates that the companion orbiting HIP 66074 is a giant planet with $m \sin i \simeq 0.8\ M_{\rm Jup}$ on an extremely elongated orbit ($e = 0.948 \pm 0.004$): only HD 20782 b, with $e = 0.97 \pm 0.01$, has a larger measured eccentricity (O'Toole et al. 2009). At periastron, the orbital separation of HIP 66074 b is just 0.04 au, making the survival of any planets in inner orbits very unlikely and further corroborating the interpretation of the 35 d periodicity as due to spot-induced rotational modulation. The K-value is much larger than that originally inferred based on the sparse HIRES RVs, which were never obtained in the vicinity of the periastron passage. This result clearly helps resolving the puzzling discrepancy with the *Gaia* orbital solution initially highlighted in the literature, but not entirely. Based on the solid evidence obtained with the HARPS-N RVs, we next investigate the specific biases present in the *Gaia*-only orbital solution.

3.3. Understanding biases in the Gaia-only solution

In order to fully reconcile the still-existing discrepancy between our RV-measured orbit and the published *Gaia* DR3 solution, we performed a set of numerical simulations. We generated a set of 140 synthetic *Gaia* astrometric observations of HIP 66074. The transit times (determined relative to the *Gaia* DR3 reference epoch $T_{\rm ref} = 2016.0$), scan angles, and along-scan parallax factors of the *Gaia* observations of HIP 66074 over the DR3 time-span were obtained from the *Gaia* Observation Forecast Tool (GOST)[4]. Each of the synthetic time–series of along-scan coordinates w was produced with the stellar motion described by the five astrometric parameters from Table A.1. The astrometric signal induced by a single companion was then added linearly, using the stellar mass value as determined in Sect. 3.1 and the orbital parameters P, T_0, e, and ω and the derived minimum mass from Sect. 3.2, varied within their respective uncertainties. The two remaining orbital elements, the orbital inclination i and the

[4] https://gaia.esac.esa.int/gost/index.jsp

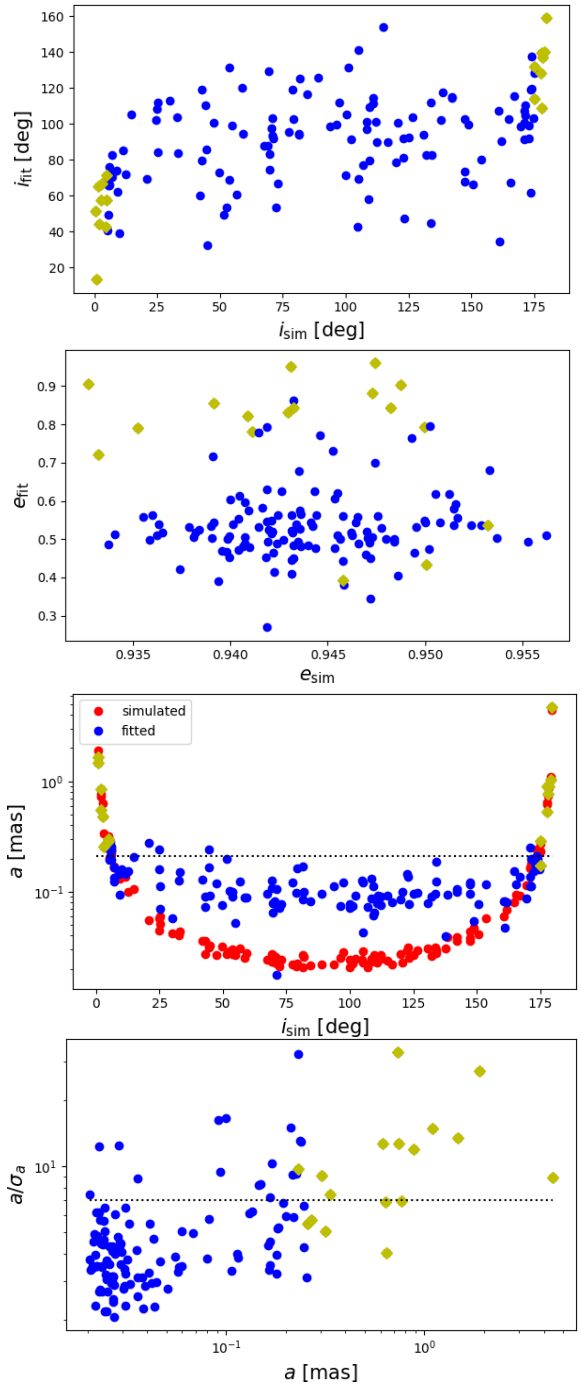

Fig. 2. *Gaia* astrometry simulations results. From top to bottom: (a) derived inclination vs. simulated value; (b) fitted eccentricity vs. simulated value; (c) derived (blue) and simulated (red) astrometric semi-major axis vs. injected orbital inclination; the black dotted line shows the semi-major axis of the *Gaia* solution, a_0; (d) significance of the $a_{\rm fit}$ vs. simulated value; the black dotted line indicates the value obtained for the *Gaia* solution. In all panels yellow diamonds highlight orbits with inclination within 5° of an exactly face-on configuration.

longitude of the ascending node Ω, were generated from uniform distributions over the $[0, \pi]$ range, and we then computed the true companion mass and angular semi-major axis based on i. Finally, the w measurements were perturbed by Gaussian random uncertainties with a standard deviation $\sigma_w = 0.1$ mas, appropriate for a star of magnitude similar to HIP 66074 for DR3-level astrometry (see Holl et al. 2023).

Each of the 140 astrometric time series was then fitted with a 12-parameter model (five astrometric parameters, seven orbital elements) using a Markov chain Monte Carlo (MCMC) algorithm, adopting the `emcee` Affine Invariant MCMC Ensemble sampler by Foreman-Mackey et al. (2013). We adopted a partly linearised Keplerian orbit model (e.g. Holl et al. 2023; Halbwachs et al. 2023). For the non-linear parameters T_0, P, e, we used uniform priors to avoid biasing the orbital solution, as illustrated in Table C.1.

The results are illustrated in the four panels of Fig. 2. As we can see, the medians and standard deviations of the fitted eccentricity and derived inclination are $e_{\rm fit} = 0.53 \pm 0.13$ and $i_{\rm fit} = 93 \pm 27°$. The combination of the intrinsically one-dimensional *Gaia* w measurements and small size of the astrometric perturbation induces a systematic underestimation of the eccentricity (an issue already hinted at by Holl et al. 2023) and a bias against close-to-face-on orbits. Furthermore, the retrieved semi-major axis is systematically overestimated, with fitted semi-major axis $a_{\rm fit} \simeq \sigma_w$, except for very small i values corresponding to simulated $a \gtrsim \sigma_w$. For quasi-face-on configurations (e.g. simulated $i \lesssim 5°$ and $i \gtrsim 175°$ for a retrograde and prograde orbits, respectively), the fitted eccentricity gets closer to the input value, but the pronounced suppression of quasi-face-on solutions remains. This bias is due to the partially linearised model fitted to noisy data, which it has already been qualitatively discussed by Gaia Collaboration (2023b). Finally, we notice that the median significance of $a_{\rm fit}/\sigma_a$ when $a \lesssim \sigma_w$ is typically around 3, well below the value of ∼7 of the published *Gaia* solution. In our simulations, this level of significance is obtained for $a \gtrsim \sigma_w$, which implies that the size of the published *Gaia* orbit is possibly correct, but it could also be overestimated by up to a factor of ∼2.

We then go on to consider that the semi-major axis of the primary (in mas) obtained by *Gaia* can be written as (Pourbaix 2001):

$$a_0 = 3.35729138 \times 10^{-5}\, P\, K\, \sqrt{1-e^2}\, \varpi / \sin i, \quad (1)$$

where K is in m s^{-1}, P in yr, and ϖ in mas. As the orbital elements from the spectroscopic orbit (including the K-value) are now robustly determined, we can make a better-informed statement on the true inclination of the orbit. If $a_0 = 0.21 \pm 0.03$ mas derived from the *Gaia* solution is correct, then this implies $i \simeq 6.5°$. If a_0 is overestimated by as much as a factor of 2, then $i \simeq 13.0°$. We cannot completely rule out the possibility of a significantly higher inclination and, therefore, a true mass closer to the minimum mass. However, this would imply (see Fig. 2) a in the range 60−25 μas for i between 25° and 90°, respectively, significantly below the quoted measurement uncertainties. It is unclear whether such a small perturbation size would have been effectively detectable in *Gaia* DR3 astrometry. We therefore conclude that the true orbit orientation indeed corresponds to a close to face-on configuration and the true mass estimate of HIP 66074b/Gaia-3b is likely in the range 3−7 $M_{\rm Jup}$ (close to the one derived by *Gaia* DR3 astrometry), fully resolving the tension between the *Gaia* solution and Doppler spectroscopy.

3.4. System architecture

HIP 66074 is known to have a faint companion, 2MASS J13324530+7459441, at an angular separation of 43.8″, as first discussed by Gomes et al. (2013). The *Gaia* DR3 astrometry firmly confirms the physical association of the two objects, albeit with a statistically significant (∼15σ) proper motion difference

$\Delta\mu$ in right ascension. Gomes et al. (2013) derived an L2 spectral type from optical spectroscopy, $T_{\rm eff} = 2080 \pm 260$ K, and bolometric luminosity $\log L/L_{\odot} = -3.78 \pm 0.045$. We took advantage of the stellar characterisation of the primary (Sect. 3.1) for further inferences. From the adopted stellar age and the models by Baraffe et al. (2015), we obtained a mass of $0.076 \pm 0.001\ M_{\odot}$ for the companion (considering the *Gaia* and near-infrared absolute magnitudes and the spectroscopic $T_{\rm eff}$; the uncertainty does not include the systematic errors of the models and the small effect of non-solar metallicity), just above the Hydrogen-burning limit. We then concluded that HIP 66074 has a very low-mass stellar companion at a projected separation of ∼1550 au.

The existence of a wide companion around a star with a planet with extreme eccentricity cannot be considered a surprise. Indeed, all the previously known planetary companions with eccentricities larger than 0.9 have further companions on wide orbits (HD 4113, Tamuz et al. 2008; HD 7449, Cheetham et al. 2018; HD 80606, Naef et al. 2001; HD 20782, Desidera & Barbieri 2007), and, more generally, a link between binary fraction and planet eccentricity has been reported (e.g. Moutou et al. 2017; Su et al. 2021). This points to a key role of dynamical interactions with an outer perturber in the generation of extreme planet eccentricities (Mustill et al. 2022). To further detail the mechanism of such interactions, we derived the timescale for the Kozai modulation, following Takeda & Rasio (2005). This is shown to be comparable to the age of the system for very high eccentricities of the outer orbit (5 Gyr for $e = 0.9$) and longer than the age of the universe at lower eccentricities (25 Gyr for $e = 0.67$). We computed γ, the angle between the separation vector and the relative velocity vector of the binary (Tokovinin & Kiyaeva 2016), finding $\gamma = 67 \pm 4°$. This indicates, in a statistical sense, a not particularly high binary eccentricity (e.g. Tokovinin & Kiyaeva 2016; Hwang et al. 2022). Furthermore, we verified both analytically (Misner et al. 1973) and via direct numerical integration that the relativistic precession timescale of the orbit is much shorter than that of the Kozai modulation, which therefore is effectively inhibited. The wide-separation low-mass stellar companion of HIP 66074 is thus unlikely to be the one responsible for the observed eccentricity of Gaia-3b. Other scenarios such as planet-planet scattering events (Carrera et al. 2019) might be more realistic scenarios for explaining this discrepancy.

4. Conclusions

We confirm the first *Gaia* astrometric planet discovery, HIP 66074b/Gaia-3b, based on new HARPS-N RV data. The object was at the centre of a much-debated, puzzling discrepancy between *Gaia* DR3 astrometry and Keck HIRES RVs of HIP 66074. Both the *Gaia* solution and HIRES RVs indicate the presence of a planetary-mass companion with a period of ∼300 days, but with entirely incompatible measurements of the astrometric orbit size and RV semi-amplitude, given the remainder of the orbital elements. This conundrum was fully resolved based solely on the critical contribution of a dense RV-monitoring with HARPS-N RV that allowed for a sampling of the periastron passage of the second-highest eccentricity gas giant ever found. In turn, based on detailed numerical simulations, this allowed the discrepancy with the *Gaia*-only solution to be reconciled. The *Gaia* orbit suffers from two main biases: the eccentricity is underestimated and the edge-on configuration is incorrect, while the true inclination angle is small, namely, $i \lesssim 13°$. The angular orbit size is likely correct or overestimated by a factor of at most ∼2. The true mass estimate of Gaia-3b, between approximately 3 and 7 $M_{\rm Jup}$, unambiguously identifies the object as a super-Jovian planet, the first-ever astrometrically detected companion fully in the planetary regime[5] to be independently confirmed by another technique after many decades of attempts (e.g. Sozzetti & de Bruijne 2018, and references therein).

Gaia-3b joins the small sample of giant exoplanets with extremely high eccentricities ($e > 0.9$), with the peculiarity that it has been found to be orbiting the star with the lowest mass star of the lot. The clearly identified wide, very-low-mass stellar companion, straddling the threshold between Deuterium- and Hydrogen-burning objects, does not appear to effectively influence the orbit of Gaia-3b via Kozai cycles, while Jovian-mass (or larger) companions out to 5−10 au are also ruled out by the lack of detectable long-term RV trends and statistically significant HIPPARCOS-*Gaia* DR3 proper motion anomaly (Kervella et al. 2022; Brandt 2021). The HIP 66074 planetary system therefore constitutes an excellent laboratory for in-depth studies on the influence of a third body and of the effects of tidal circularisation on the parameters of the exoplanet Gaia-3b. Further investigations of the system are warranted and these will benefit from the effective combination of RVs and *Gaia* time-series astrometry spanning 5.5 years, when the next major data release, DR4, is published near the end of 2025.

Acknowledgements. This work has made use of data from the European Space Agency (ESA) mission *Gaia* (https://www.cosmos.esa.int/gaia), processed by the *Gaia* Data Processing and Analysis Consortium (DPAC, https://www.cosmos.esa.int/web/gaia/dpac/consortium). Funding for the DPAC has been provided by national institutions, in particular the institutions participating in the *Gaia* Multilateral Agreement. We acknowledge the financial support from the agreement ASI-INAF n.2018-16-HH.0, and from the Italian Space Agency (ASI) under contract 2018-24-HH.0 "The Italian participation to the *Gaia* Data Processing and Analysis Consortium (DPAC)" in collaboration with the Italian National Institute of Astrophysics. M.P. acknowledges the financial support from the ASI-INAF Addendum n.2018-24-HH.1-2022 "Partecipazione italiana al *Gaia* DPAC – Operazioni e attività di analisi dati". This work has made use of the SIMBAD and VizieR databases and catalogue access tool at the CDS, Strasbourg (France), and NASA's Astrophysics Data System Bibliographic Services. This Letter includes data collected with the TESS mission, obtained from the MAST data archive at the Space Telescope Science Institute (STScI). Funding for the TESS mission is provided by the NASA Explorer Program. STScI is operated by the Association of Universities for Research in Astronomy, Inc., under NASA contract NAS 5-26555.

References

Adibekyan, V. Z., Delgado Mena, E., Sousa, S. G., et al. 2012, A&A, 547, A36
Ambikasaran, S., Foreman-Mackey, D., Greengard, L., Hogg, D. W., & O'Neil, M. 2015, IEEE Trans. Pattern Anal. Mach. Intell., 38, 252
Anders, F., Khalatyan, A., Queiroz, A. B. A., et al. 2022, A&A, 658, A91
Anglada-Escudé, G., & Butler, R. P. 2012, ApJS, 200, 15
Astudillo-Defru, N., Delfosse, X., Bonfils, X., et al. 2017, A&A, 600, A13
Bailer-Jones, C. A. L., Rybizki, J., Fouesneau, M., Demleitner, M., & Andrae, R. 2021, AJ, 161, 147
Baraffe, I., Homeier, D., Allard, F., & Chabrier, G. 2015, A&A, 577, A42
Biazzo, K., Randich, S., & Palla, F. 2011, A&A, 525, A35
Biazzo, K., D'Orazi, V., Desidera, S., et al. 2022, A&A, 664, A161
Brandt, T. D. 2021, ApJS, 254, 42
Brewer, J. M., Fischer, D. A., Valenti, J. A., & Piskunov, N. 2016, ApJS, 225, 32
Buchner, J., Georgakakis, A., Nandra, K., et al. 2014, A&A, 564, A125
Butler, R. P., Vogt, S. S., Laughlin, G., et al. 2017, AJ, 153, 208
Carrera, D., Raymond, S. N., & Davies, M. B. 2019, A&A, 629, L7
Castelli, F., & Kurucz, R. L. 2003, in Modelling of Stellar Atmospheres, eds. N. Piskunov, W. W. Weiss, & D. F. Gray, 210, A20

[5] In the recent discoveries of the directly imaged planetary companions AF Lep b (Mesa et al. 2023) and HIP 99770 b (Currie et al. 2023), the detection of an astrometric acceleration based on HIPPARCOS-*Gaia* absolute astrometry alone only allows us to place lower limits to the ratio M/a^2.

Cheetham, A., Ségransan, D., Peretti, S., et al. 2018, A&A, 614, A16
Cosentino, R., Lovis, C., Pepe, F., et al. 2012, in Ground-based and Airborne Instrumentation for Astronomy IV, eds. I. S. McLean, S. K. Ramsay, & H. Takami, SPIE Conf. Ser., 8446, 84461V
Covino, E., Esposito, M., Barbieri, M., et al. 2013, A&A, 554, A28
Currie, T., Brandt, G. M., Brandt, T. D., et al. 2023, Science, 380, 198
Cutri, R. M., Skrutskie, M. F., van Dyk, S., et al. 2003, VizieR Online Data Catalog: II/246
Cutri, R. M., Wright, E. L., Conrow, T., et al. 2021, VizieR Online Data Catalog: II/328
Damasso, M., Sozzetti, A., Lovis, C., et al. 2020, A&A, 642, A31
Desidera, S., & Barbieri, M. 2007, A&A, 462, 345
Desidera, S., Sozzetti, A., Bonomo, A. S., et al. 2013, A&A, 554, A29
Eastman, J. 2017, Astrophysics Source Code Library [record ascl:1710.003]
Eastman, J. D., Rodriguez, J. E., Agol, E., et al. 2019, ArXiv e-prints [arXiv:1907.09480]
Feroz, F., Hobson, M. P., Cameron, E., & Pettitt, A. N. 2019, Open J. Astrophys., 2, 10
Foreman-Mackey, D., Hogg, D. W., Lang, D., & Goodman, J. 2013, PASP, 125, 306
Gaia Collaboration (Vallenari, A., et al.) 2023a, A&A, 674, A1
Gaia Collaboration (Arenou, F., et al.) 2023b, A&A, 674, A34
Gomes, J. I., Pinfield, D. J., Marocco, F., et al. 2013, MNRAS, 431, 2745
Gruner, D., Barnes, S. A., & Weingrill, J. 2023, A&A, 672, A159
Gustafsson, B., Edvardsson, B., Eriksson, K., et al. 2008, A&A, 486, 951
Halbwachs, J.-L., Pourbaix, D., Arenou, F., et al. 2023, A&A, 674, A9
Henden, A. A., Templeton, M., Terrell, D., et al. 2016, VizieR Online Data Catalog: II/336
Høg, E., Fabricius, C., Makarov, V. V., et al. 2000, A&A, 355, L27
Holl, B., Sozzetti, A., Sahlmann, J., et al. 2023, A&A, 674, A10
Hwang, H.-C., Ting, Y.-S., & Zakamska, N. L. 2022, MNRAS, 512, 3383
Kervella, P., Arenou, F., & Thévenin, F. 2022, A&A, 657, A7
Lindegren, L., Klioner, S. A., Hernández, J., et al. 2021, A&A, 649, A2
Marcussen, M. L., & Albrecht, S. H. 2023, AJ, 165, 266
Mesa, D., Gratton, R., Kervella, P., et al. 2023, A&A, 672, A93
Misner, C. W., Thorne, K. S., & Wheeler, J. A. 1973, Gravitation (San Francisco: W.H. Freeman and Company)
Montes, D., López-Santiago, J., Gálvez, M. C., et al. 2001, MNRAS, 328, 45
Moutou, C., Vigan, A., Mesa, D., et al. 2017, A&A, 602, A87
Mustill, A. J., Davies, M. B., Blunt, S., & Howard, A. 2022, MNRAS, 509, 3616
Naef, D., Latham, D. W., Mayor, M., et al. 2001, A&A, 375, L27
Nardiello, D., Malavolta, L., Desidera, S., et al. 2022, A&A, 664, A163
O'Toole, S. J., Tinney, C. G., Jones, H. R. A., et al. 2009, MNRAS, 392, 641
Perger, M., García-Piquer, A., Ribas, I., et al. 2017, A&A, 598, A26
Piskunov, N., & Valenti, J. A. 2017, A&A, 597, A16
Pourbaix, D. 2001, A&A, 369, L22
Sneden, C. 1973, ApJ, 184, 839
Sozzetti, A., & de Bruijne, J. 2018, in Handbook of Exoplanets, eds. H. J. Deeg, & J. A. Belmonte, 81
Stassun, K. G., & Torres, G. 2016, AJ, 152, 180
Su, X.-N., Xie, J.-W., Zhou, J.-L., & Thebault, P. 2021, AJ, 162, 272
Takeda, G., & Rasio, F. A. 2005, ApJ, 627, 1001
Tamuz, O., Ségransan, D., Udry, S., et al. 2008, A&A, 480, L33
Tokovinin, A., & Kiyaeva, O. 2016, MNRAS, 456, 2070
Winn, J. N. 2022, AJ, 164, 196
Yi, S., Demarque, P., Kim, Y.-C., et al. 2001, ApJS, 136, 417
Zacharias, N., Finch, C. T., Girard, T. M., et al. 2012, VizieR Online Data Catalog: I/322A
Zechmeister, M., & Kürster, M. 2009, A&A, 496, 577

[1] INAF – Osservatorio Astrofisico di Torino, Via Osservatorio 20, 10025 Pino Torinese, Italy
e-mail: alessandro.sozzetti@inaf.it
[2] INAF – Osservatorio Astronomico di Padova, Vicolo dell'Osservatorio 5, 35122 Padova, Italy
[3] INAF – Osservatorio Astronomico di Roma, Via Frascati 33, 00078 Monte Porzio Catone, Roma, Italy
[4] INAF – Osservatorio Astrofisico di Catania, Via S. Sofia 78, 95123 Catania, Italy
[5] Dipartimento di Fisica e Astronomia "G. Galilei" – Università degli Studi di Padova, Vicolo dell'Osservatorio 3, 35122 Padova, Italy
[6] INAF – Osservatorio Astronomico di Palermo, Piazza del Parlamento 1, 90134 Palermo, Italy
[7] INAF – Osservatorio Astronomico di Trieste, Via Tiepolo 11, 34143 Trieste, Italy
[8] INAF – Osservatorio Astronomico di Brera, Via E. Bianchi 46, 23807 Merate, LC, Italy
[9] Fundación Galileo Galilei – INAF, Rambla José Ana Fernandez Pérez 7, 38712 Breña Baja, TF, Spain
[10] Dipartimento di Fisica, Università degli Studi di Torino, Via Pietro Giuria 1, 10125 Torino, Italy
[11] INAF – Osservatorio Astronomico di Capodimonte, Salita Moiariello 16, 80131 Napoli, Italy
[12] Department of Physics, University of Rome "Tor Vergata", Via della Ricerca Scientifica 1, 00133 Rome, Italy
[13] Max Planck Institute for Astronomy, Königstuhl 17, 69117 Heidelberg, Germany
[14] INAF – Osservatorio Astronomico di Cagliari, Via della Scienza 5, 09047 Selargius, CA, Italy
[15] Dipartimento di Fisica & Astronomia, Università di Firenze, Largo Enrico Fermi 5, 50125 Firenze, Italy

Appendix A: Stellar parameters

We report in Table A.1 the main astrometric, photometric, and spectroscopic stellar parameters of HIP 66074. Only broad-band photometry effectively used in the paper for the SED fit is listed.

Table A.1. Astrometry, photometry, and spectroscopically derived stellar properties of HIP 66074.

HIP 66074, GJ 9452, TYC 4558-1471-1		
Parameter	Value	Refs.
Astrometry:		
α (J2000)	13:32:41.01	[1,2]
δ (J2000)	+75:00:24.80	[1,2]
μ_α [mas yr^{-1}]	-440.558 ± 0.015	[1,2]
μ_δ [mas yr^{-1}]	49.539 ± 0.012	[1,2]
ϖ [mas]	28.24 ± 0.01	[1,2]
d [pc]	$35.37^{+0.03}_{-0.02}$	[3]
Photometry:		
B_T [mag]	11.673 ± 0.073	[4]
V_T [mag]	10.446 ± 0.041	[4]
B_J [mag]	11.468 ± 0.033	[5,6]
V_J [mag]	10.181 ± 0.117	[5,6]
$i_{\rm sdss}$ [mag]	9.218 ± 0.070	[5,6]
J [mag]	7.910 ± 0.024	[7]
H [mag]	7.302 ± 0.033	[7]
K_s [mag]	7.182 ± 0.016	[7]
$W1$ [mag]	7.054 ± 0.049	[8]
$W2$ [mag]	7.189 ± 0.020	[8]
$W3$ [mag]	7.133 ± 0.016	[8]
$W4$ [mag]	7.079 ± 0.085	[8]
Stellar Parameters:		
$T_{\rm eff}$ [K]	4300 ± 60	[9]
$\log g$ [dex]	4.58 ± 0.06	[9]
[Fe/H] [dex]	0.12 ± 0.05	[9]
$M_\star$ [M$_\odot$]	$0.705^{+0.025}_{-0.023}$	[9]
$R_\star$ [R$_\odot$]	$0.690^{+0.013}_{-0.012}$	[9]
$\varrho_\star$ [g cm^{-3}]	$3.02^{+0.18}_{-0.17}$	[9]
$L_\star$ [L$_\odot$]	$0.152^{+0.006}_{-0.006}$	[9]
$v \sin i_\star$ [km s^{-1}]	1.8 ± 0.6	[9]
$< \log R'_{HK} >$	-4.80 ± 0.04	[9]
t [Gyr]	$7.9^{+4.9}_{-4.1}$	[9]

References. [1] Gaia Collaboration 2023a; [2] Lindegren et al. 2021; [3] Bailer-Jones et al. 2021; [4] Høg et al. 2000; [5] Zacharias et al. 2012; [6] Henden et al. 2016; [7] Cutri et al. 2003; [8] Cutri et al. 2021; [9] this work.

Appendix B: Photometry

Figure B.1 shows the results of the SED fit to the broad-band photometric data available for HIP 66074. Figure B.2 shows the TESS light curve along with a GLS periodogram analysis of various sector subsets.

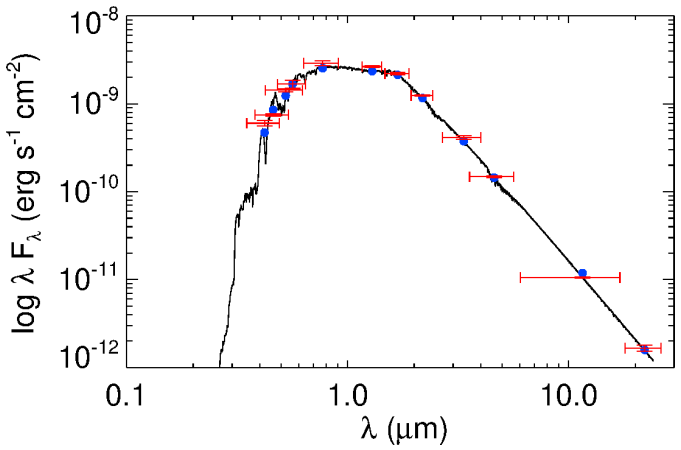

Fig. B.1. Spectral energy distribution of HIP 66074. Red markers depict the photometric measurements with vertical error bars corresponding to the reported measurement uncertainties from the catalogue photometry. Horizontal error bars depict the effective width of each pass-band. The black curve corresponds to the most likely stellar atmosphere model. Blue circles depict the model fluxes over each pass-band.

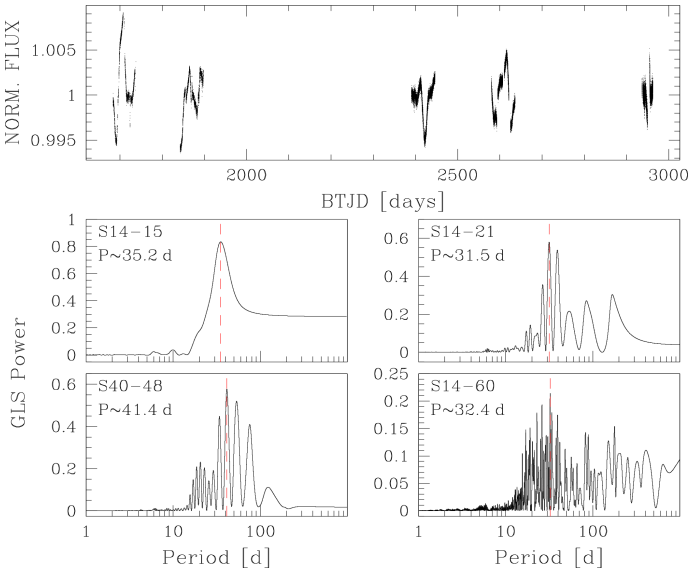

Fig. B.2. TESS photometry and periodogram analysis. Top panel: TESS light curve of HIP 66074 in the nine available sectors. Time is expressed in TESS Barycentric Julian Day (BTJD), i.e. JD - 2457000.0 and corrected to the arrival times at the barycenter of the Solar System. Central and bottom panels: GLS periodograms of different sector subsets as well as of the full dataset (bottom right panel). The vertical red dashed line indicates the period of the highest periodogram peak.

Appendix C: Gaia astrometry simulations

Table C.1 lists the priors adopted for the non-linear parameters in the orbital fits to the synthetic Gaia time series carried out with `emcee`.

Table C.1. Priors on P, e and T_0 in the analysis of the Gaia astrometry simulations.

Parameter	Prior
$T0$ [yr$-T_{\rm ref}$]	$\mathcal{U}(-0.1, 0.8)$
P [yr]	$\mathcal{U}(0.1, 2.)$
e	$\mathcal{U}(0, 1)$

Appendix D: HARPS-N Spectroscopy

Table D.1 lists the TERRA-extracted HARPS-N RV data and their uncertainties, along with the time series of the $S_{\rm MW}$ spectroscopic activity indicator. Figure D.1 shows GLS periodograms of the HARPS-N RV residuals to a single Keplerian fit and of the S-index time-series.

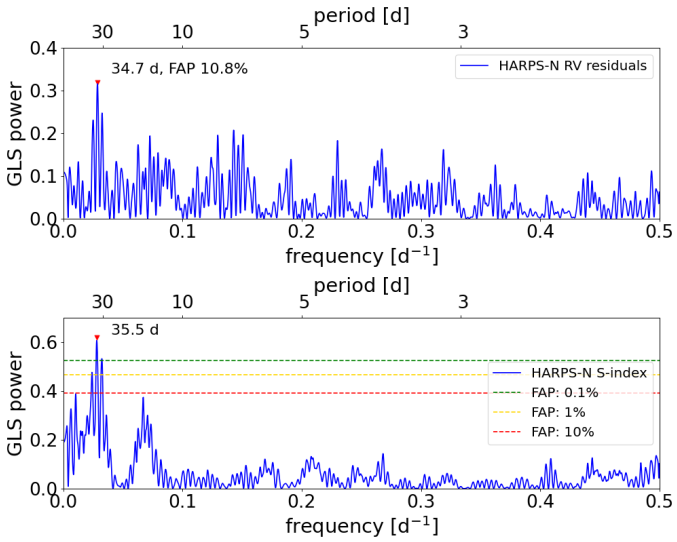

Fig. D.1. GLS periodogram of the residuals to a Keplerian fit of the HARPS-N RVs alone (top). GLS periodogram of the $S_{\rm MW}$ time-series (bottom).

Table D.1. HARPS-N RVs and $S_{\rm MW}$ time-series of HIP 66074.

BJD$_{\rm UTC}$ $-2\,400\,000$	RV (m s^{-1})	$\pm1\sigma$ (m s^{-1})	$S_{\rm MW}$	$\pm1\sigma$
59735.46728	6.6	1.8	0.848	0.030
59737.41484	-1.4	1.6	0.787	0.036
59738.48208	-0.5	1.5	0.779	0.029
59739.44066	-1.1	3.9	0.753	0.094
59747.42280	2.9	0.9	0.820	0.013
59748.46935	3.2	1.3	0.830	0.025
59749.49472	3.5	1.9	0.885	0.032
59750.46476	4.6	1.4	0.824	0.022
59751.45070	4.0	0.9	0.833	0.011
59752.44196	2.2	1.1	0.821	0.017
59768.40750	-5.9	0.8	0.710	0.011
59769.38927	-2.3	2.0	0.744	0.043
59770.39791	-1.3	1.0	0.716	0.017
59771.39447	-1.3	1.1	0.742	0.020
59772.43652	-0.2	0.8	0.741	0.009
59773.41055	2.1	0.8	0.756	0.008
59774.39651	-1.9	1.0	0.731	0.013
59775.40448	-3.3	1.1	0.785	0.017
59788.38730	-2.8	1.1	0.793	0.018
59789.41025	0.1	1.7	0.815	0.036
59792.40137	-0.7	1.2	0.819	0.025
59801.38146	-6.1	1.2	0.718	0.027
59802.37484	-8.1	0.9	0.742	0.011
59950.72695	-36.4	1.3	0.731	0.021
59951.78744	-36.7	0.9	0.764	0.014
59952.78148	-40.2	1.2	0.776	0.020
59954.74393	-47.2	2.0	0.733	0.055
59959.75447	-78.6	1.5	0.784	0.030
59962.78575	-130.2	1.2	0.761	0.024
59963.76959	-39.5	1.3	0.784	0.034
59973.75112	3.9	1.7	0.714	0.034
59977.61034	3.7	1.6	0.684	0.037
59978.65445	-1.2	1.8	0.685	0.043
59983.71256	4.4	1.1	0.731	0.020
59996.69507	7.8	1.2	0.823	0.027
59998.68966	5.8	0.9	0.798	0.012
60002.71664	3.4	1.1	0.760	0.016
60005.63687	1.7	0.9	0.787	0.013
60006.66129	0.3	1.1	0.823	0.018
60007.64068	2.0	1.0	0.776	0.012
60008.70783	1.9	0.9	0.812	0.017
60021.61256	1.8	1.5	0.753	0.030
60022.65402	3.4	1.4	0.743	0.024
60030.60416	2.5	1.2	0.840	0.023
60031.59621	0.0	1.0	0.836	0.020
60033.60929	-3.0	2.4	0.882	0.063
60034.54573	-0.6	1.5	0.836	0.031
60035.63139	3.7	1.6	0.804	0.032
60037.62247	0.4	1.4	0.809	0.023
60038.65011	1.7	1.8	0.830	0.038
60041.53353	-2.3	1.1	0.758	0.016
60042.61339	-1.6	1.3	0.777	0.027
60045.62151	-10.5	3.1	0.931	0.094
60046.57693	-1.5	2.5	0.760	0.067
60047.54405	-4.3	6.3	0.782	0.218
60048.56007	0.1	1.3	0.806	0.025
60049.52530	-0.3	1.0	0.761	0.018
60051.49598	5.5	1.8	0.808	0.035
60064.53843	1.4	1.2	0.795	0.024
60065.45549	3.1	1.0	0.793	0.017

Appendix E: Orbital fits Posteriors and stellar activity model

Figures E.1 and E.2 show the HARPS-N RV residuals (i.e. after subtracting the Keplerian for planet b) together with the GP QP best-fit solution for the RV signal of stellar origin and the joint posterior distributions of all the model parameters in the case of a single-Keplerian + GP orbital fits, respectively.

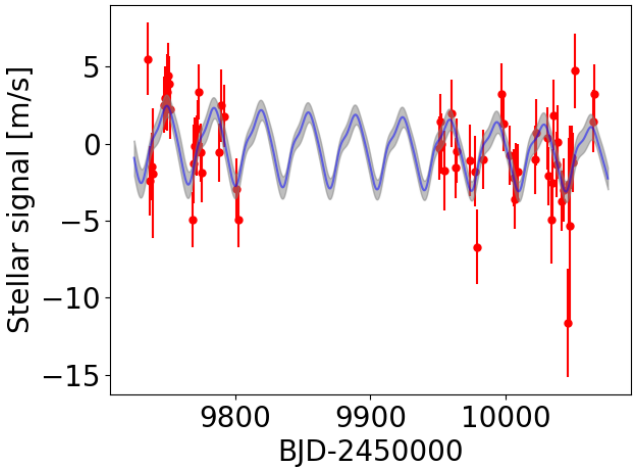

Fig. E.1. HARPS-N RV time-series after subtraction of the best-fit orbital model for planet b, showing the correlated signal related to variations in stellar activity.

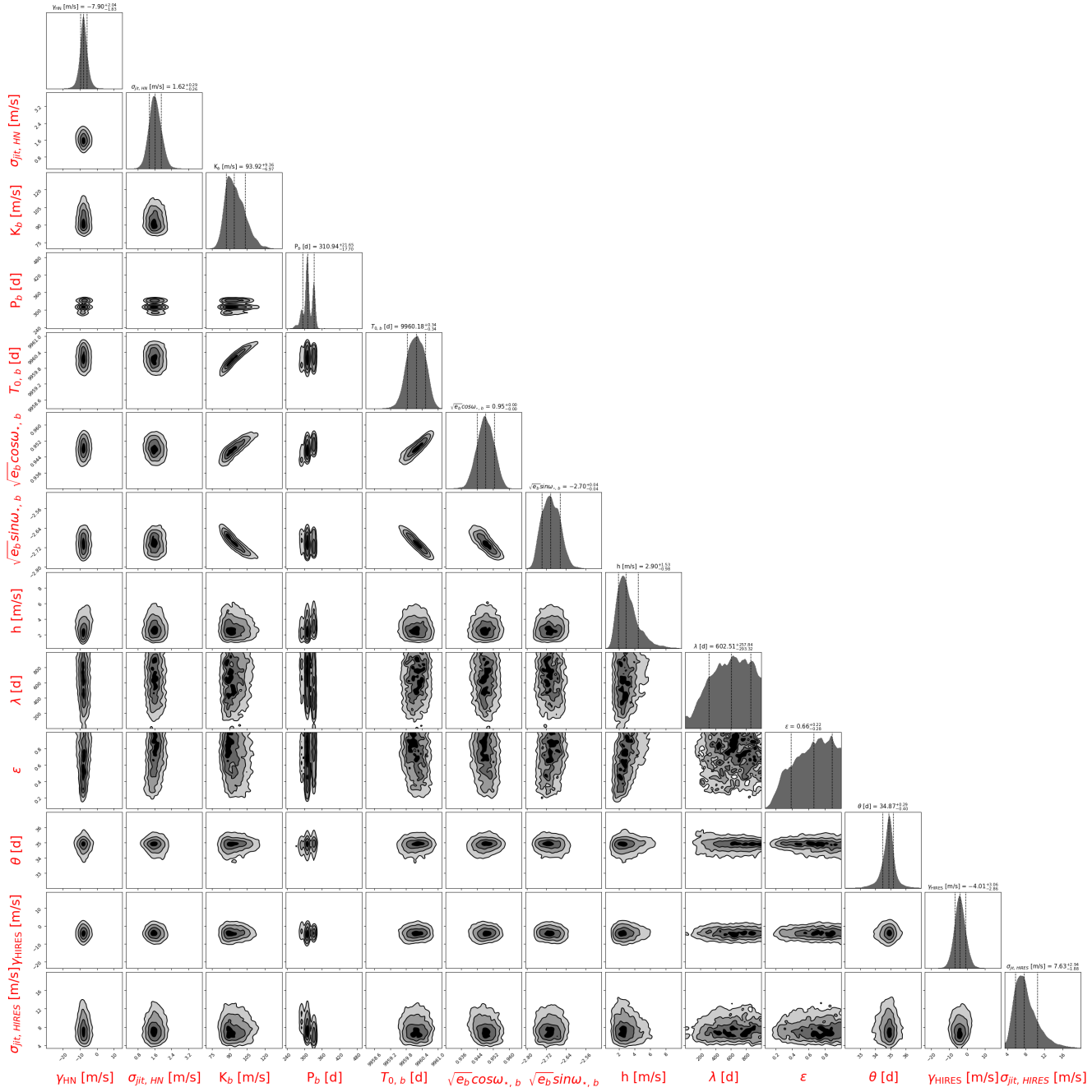

Fig. E.2. Posterior distributions of the model (hyper)parameters of our assumed best-fit model, including a Keplerian for planet b and a GP quasi-periodic correlated stellar activity signal fitted to the HARPS-N RVs of HIP 66074.